Research article

An effective QUATRE algorithm based on reorganized mechanism and its application for parameter estimation in improved photovoltaic module

Fei-Fei Liu [a], Shu-Chuan Chu [a,c,*], Chia-Cheng Hu [b], Junzo Watada [e], Jeng-Shyang Pan [a,d]

[a] *College of Computer Science and Engineering, Shandong University of Science and Technology, Qingdao, 266590, China*
[b] *College of Artificial Intelligence, Yango University, Fuzhou, 350015, China*
[c] *College of Science and Engineering, Flinders University, 1284 South Road, Tonsley, SA 5042, Australia*
[d] *Department of Information Management, Chaoyang University of Technology, Taichung, 413310, Taiwan*
[e] *Waseda University, 2-7 Hibikino, Wakamatsu-ku, Kitakyushu, Fukuoka, 808-0135, Japan*

A R T I C L E   I N F O

A B S T R A C T

The traditional parameter estimation methods for photovoltaic (PV) module are strictly limited by the reference standards. On the basis of the double diode model (DDM), this paper proposes a modified PV module that is independent of the reference conditions and can be used for the transformation and reconfiguration of PV module. With respect to the issue of the slow convergence precision and the tendency to trap in the local extremum of the QUATRE algorithm, this research incorporates the QUATRE algorithm with recombination mechanism (RQUATRE) to tackle the problem of parameter estimation for the improved PV modules described above. Simulation data show that the RQUATRE wins 29, 29, 21, 17 and 15 times with the FMO, PIO, QUATRE, PSO and GWO algorithms on the CEC2017 test suite. In addition, in a modified PV module for the parameter extraction problem, the final experimental results achieved a value of 2.99×10^{-3} at RMSE, all better than the accuracy values of the compared algorithms. In the fitting process of IAE, the final values are also all less than 10%, which can satisfy the fitting needs.

1. Introduction

With the evolution of era, the high consumption of fossil fuels has led to environmental pollution and a growing demand for clean and sustainable renewable energy sources [1]. In this regard, with its huge reserves and lack of environmental pollution, photovoltaic power is a prospective alternative energy source. At the heart of solar energy systems lies the photovoltaic (PV) module [2]. However, the effectiveness of modules can be dramatically affected depend on various factors related to the environment, including ambient temperature [4], humidity, solar radiation intensity, and dust accumulation. Therefore, PV modules play a critical role in obtaining relevant information about the internal conditions of the modules, which can be used to accurately calculate their energy output and address other issues.

---

* Corresponding author. College of Computer Science and Engineering, Shandong University of Science and Technology, Qingdao, 266590, China.
E-mail address: scchu0803@gmail.com (S.-C. Chu).

For the PV [5,6] modules to continuously produce energy at maximum power output, the generator must be kept in the maximum power point tracking (MPPT) [7]. It is necessary to adjust each parameter within the system with respect to the influence of the environmental humidity and the intensity of solar radiation on the power generation [8]. MPPT-based techniques rely on PV module parameters as system input to achieve more efficient and accurate maximum power tracking [9,10]. Moreover, when building a solar cell model, stable energy output and effective maximum power tracking must be taken into account during the calculation of current and voltage. However, outdoor PV modules are significantly affected by ambient temperature, solar radiation intensity and dust shading on the module surface. It made the construction of an accurate and simply calculated PV module at different ambient temperatures and solar radiation intensities a challenging task. Experts and scholars have proposed diverse opinions on PV module modeling approaches.

Various models have been proposed in literature for constructing PV modules, including the single-diode model (SDM) [11,12], double-diode model (DDM) [13,14], and three-diode model (TDM) [15]. These circuit models are designed to accurately represent the electrical behavior of the modules under specific conditions. However, constructing circuit models that accurately reflect the real conditions has not yet been achieved. Therefore, accurate estimation of the parameters of PV modules remains a key research area.

Pan et al. proposed a method for parameter extraction using true-case data when occlusion is present [16]. Tian et al. proposed a method for maximizing power tracking under different coverage scenarios [17]. Jately et al. established a general equation to determine the optimal digitization step in duty cycle-based perturbations, specifically for the observation algorithm in low irradiance conditions [18]. Li et al. introduced an innovative Overall Distribution (OD) MPPT algorithm that quickly searches the vicinity of global maximum power points and integrates with the Particle Swarm Optimization (PSO) MPPT algorithm to enhance its precision [19].

Industrial optimization is crucial for enhancing the efficiency of industrial processes. In the generation of electricity, it plays a significant role in powering other industrial activities. The optimization processes of the equivalent circuit model in the PV module that involves a multitude of processes that culminate in considerable power optimization. Due to the varied parameters affecting the space of the battery, the optimization procedure is non-linear. Therefore, it is paramount to establish a PV module model that can swiftly estimate the internal parameter information in diverse operating conditions to predict the MPPT using I-V curve characteristics under different PV module models.

Many researchers have focused on DDM as a research topic due to its ability to precisely forecast the internal properties of thermal photovoltaic cell in low irradiation conditions, which ensures accurate parameter estimation of PV systems under appropriate conditions. To obtain more precise parameter information in actual environments, the estimation of parameters of the models for different solar radiation intensities and temperatures is essential. The traditional parameter estimation method for different working conditions involves two stages. Firstly, the mechanical parameter is estimated with references conditions. Secondly, parameter information is calculated under different ambient temperatures and solar radiation intensities using a calculation method that considers the dependence of physical parameters within the impact of photovoltaic components on external conditions. Therefore, selection from the reference circumstance can impact the final calculation outcome.

Since the manufacturers of PV modules do not give the parameter information of DDM at the factory, and some instruments cannot obtain the parameter information, there are many ways to measure the amount of parameter information inside the PV modules. Manufactures and sellers will only collect the operating data, open circuit voltage (V_{oc}) [20], short circuit current (I_{sc}) [21], I_{mm} and V_{mm} represent current and voltage at the point of maximum power of each PV system sold. These data can be utilized to estimate parameters for cells at standard test conditions (STC) [22] with a radiation intensity of $1000 \text{W}/\text{m}^2$ and a cell temperature of $25\,^{\circ}\text{C}$, and then use the estimated parameter information to provide a basis for other calculation processes of PV module. These estimation methods can be categorized into numerical calculation methods [23,24] and analytical methods [25–27]. Numerical methods use an iterative process such as gradient descent to solve the mathematical equations that make up the model to estimate parameters. However, the accuracy of the solution obtained by the numerical calculation methods relies on both the selection of initial values and the number of parameters to estimate, making it time-consuming and computationally expensive. Analytical methods, on the other hand, are often simpler and more practical. They rely on approximations to determine the model parameter information based on actual data. While the approximation process may decrease the accuracy of PV module parameter estimation, these traditional methods are limited to estimating parameters under STC conditions.

Based on the data measured from the I-V characteristic curve, heuristic algorithms can estimate the parameter information inside the model more accurately. Some of the more commonly used algorithms are: Particle Swarm Optimization (PSO) [28,29], QUasi-Affine TRansformation Evolution Algorithm (QUATRE) [30,31], Pigeon-inspired Optimization (PIO) [16], Genetic Algorithm (GA) [32], Fish Migration Optimization (FMO) [33], Dragonfly Algorithm (DA) [34,35], Grey Wolf Optimization algorithm (GWO) [36], Artificial Bee Colony Algorithm (ABC) [37], Gannet optimization algorithm (GOA) [38], Colony Predation Algorithm (CPA) [39, 40], Whale Optimization Algorithm (WOA) [41], Bamboo Forest Growth Optimization Algorithm (BFGO) [42], Water Cycle Algorithm (WCA) [43]. Heuristic algorithms have an advantage over traditional analytical and numerical calculation methods in that they do not rely on a specific choice of initial values and are known for providing higher accuracy in estimating parameters.

To estimate the parameter information within a PV module and calculate its output power under different test circumstances, just like different sun radiation or ambient temperature, parameters estimated from STC need to be translated. While there are several methods available for estimating PV module performance under diverse working conditions, there remain some challenges. One of the significant challenges is the inability to determine the influence of environmental factors on the DDM's physical parameters.

As the level of solar irradiation increases, the ideality factor of the diode undergoes continuous changes. Some researchers suggest that the ideality factor varies depending on the working conditions. Currently, many formulas lack a sound theoretical basis, and some
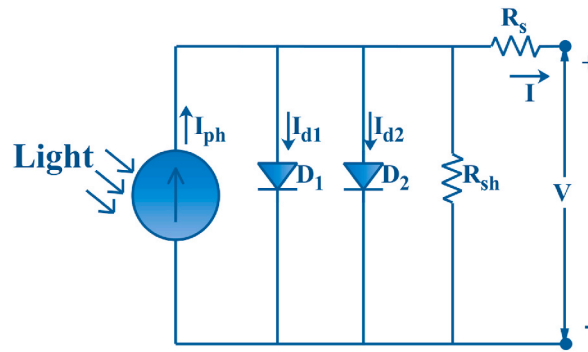
Fig. 1. The equivalency electric circuity model diagram of DDM.

rely on oversimplified assumptions. Additionally, the estimation of the final number of parameters may be affected by the working environment of the selected test condition. Many studies in the literature have opted to work under STC conditions.

This paper introduces a new approach for parameter estimation under various working conditions. A parameter estimation method based on a mathematical model is used for reconstruction and correction. The real measurement data is compared with the calculated data, and the root mean square error (*RMSE*) is minimized. The heuristic algorithm is applied in this paper as a method to tackle on this issue. The improved PV module model will increase the dimensionality and calculation, but the method will be applicable to various working situations and has strong generalizability.

The remainder of this paper is structured as follows: Section 2 provides a description of the mathematical modeling and problem optimization for the PV module model used in this paper. Section 3 focuses on the reconstruction and improvement of the relationship between the double-diode model and the environment. It aims to render the model parameters independent of solar temperature and irradiance. Section 4 presents the evaluation criteria for model parameter estimation, such as the objective optimization function. Section 5 introduces an effective QUATRE algorithm based on reorganized mechanism (RQUATRE). The parameter estimation results of the PV module based on the DDM are analyzed and compared with various heuristic algorithms on the CEC2017 test suite in Section 6. The conclusions and the prospects for future research are given in Section 7.

The contributions of the work of this paper are:

1. An effective QUATRE algorithm based on reorganized mechanism (RQUATRE) is proposed, which can prevent the algorithm from getting trapped in the local optimum pitfall and enhance the performance of exploration of the search space.
2. On the CEC2017 test suite, RQUATRE is experimentally comparing with five of the most advanced evolutionary algorithms. The experimental data indicate that RQUATRE outperforms other comparative algorithms.
3. In this paper, the conventional PV module model is reconstructed to enhance the versatility under various operating conditions, and then the parameters of the improved model are estimated by the RQUATRE algorithm. The traditional PV module needs to estimate seven parameters, while the improved PV module used in this paper needs to estimate eighteen parameters. Although the number of parameters will increase, the estimation accuracy will be greatly improved. Simulation experiments also show that the parameters estimated by the RQUATRE algorithm have higher accuracy.

2. The model for photovoltaic module with DDM

2.1. Theoretical mathematical basis modeling DDM

DDM is frequently used as a reference model in solar energy performance analysis and parameter estimation due to its ability to accurately reflect the output characteristics of PV modules in low-irradiation environments. It follows circuit laws and the I-V curve characteristics of its equivalent circuit model can be determined using Kirchhoff's law [44] as shown in Eq. (1). The equivalency electric circuity model diagram is shown in Fig. 1.

$$I = I_{ph} - \frac{V + IR_s}{R_{sh}} - I_0 \left[e^{\frac{V+IR_s}{V_{t1}}} - 1 \right] - I_1 \left[e^{\frac{V+IR_s}{V_{t2}}} - 1 \right] \tag{1}$$

The equation above shows that the output current and voltage of the model are represented by I and V. I_{ph} is the current generated by the photosensitive device inside the equivalent circuit, R_s and R_{sh} are the equivalent circuit with resistance in series and in parallel. I_{d1} and I_{d2} are current flowing through two double diodes. I_0 represents saturation current, I_1 is diffusion current. V_{t1} and V_{t2} represent the calculated voltage at a certain temperature. These two values depend greatly on the temperature, which is expressed in the specific computational expression as Eq. (2).
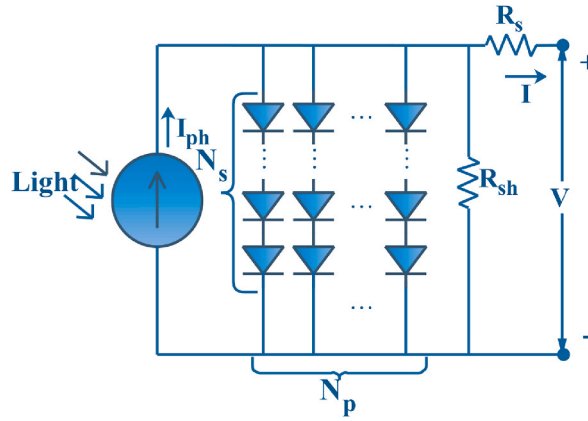
Fig. 2. The equivalency electric circuity model diagram of the PV module.

Table 1
Transformation patterns of photovoltaic module parameters.

Item.	Description	Internal params for N_s cells connected in series	Internal params for the parallel connection of N_p cells
1.	I_{ph}	I_{ph}	$N_p I_{ph}$
2.	V_t	$N_s V_t$	V_t
3.	R_s	$N_s R_s$	R_s/N_p
4.	R_{sh}	$N_s R_{sh}$	R_{sh}/N_p

$$
\begin{cases}
V_{t1} = \dfrac{n_1 kT}{q} \\[2mm]
V_{t2} = \dfrac{n_2 kT}{q}
\end{cases}
\tag{2}
$$

Eq. (2) involves various parameters, such as k, which signifies the Boltzmann constant (valued at $1.381 \times 10^{-23}\,\mathrm{J}/K$), q indicates the charge amount (valued at $1.602 \times 10^{-19}\mathrm{C}$), and T denotes the ambient temperature of the DDM, usually measured in Calvin. Additionally, n_1 and n_2 represent two diode's ideality factors, the ideal coefficient of each diode may be slightly different due to the uniqueness of each blade.

2.2. PV module model

The mathematical model of PV module is similar to DDM. It consists of a series of different arrays of $N_s * N_p$ connected by the series and parallel lines. Fig. 2 displays the equivalency electric circuity model diagram of the PV module. The relationship between DDM and PV module is shown in Table 1. It is displayed in the physical presentation as in Eq. (3). This paper focuses on carrying out parameter estimation for the PV module employing the DDM.

$$
I = N_p I_{ph} - N_p I_0 \left[\exp\left(\frac{1}{V_{t1}} \left(\frac{V}{N_s} + \frac{IR_s}{N_p} \right) \right) - 1 \right] - N_p I_1 \left[\exp\left(\frac{1}{V_{t2}} \left(\frac{V}{N_s} + \frac{IR_s}{N_p} \right) \right) - 1 \right] - \frac{N_p}{R_p} \left(\frac{V}{N_s} + \frac{IR_s}{N_p} \right)
\tag{3}
$$

In Eq. (1), the estimation and optimization process of seven parameters $A = (I_{ph}, I_0, I_1, R_s, R_{sh}, n_1, n_2)$ is included. The precision and effectiveness of the model are greatly influenced by the values of the seven parameters. Precisely and promptly obtaining information about these parameters can enhance the performance of the chosen model.

Based on the measured values of current I and voltage V, seven parameters of the PV module are calculated for different working environments. The model given by Eq. (1) is the mathematical representation under STC conditions. In the test environment under non-STC conditions. The model is not applicable. Eqs. (4)–(10) modify and reconstruct the model that is only suitable for STC environment can work at different temperatures and solar radiation intensities, which improves the universality of the model. This paper considers the dependence of physical parameters I_{ph}, R_s, n_1, n_2 and R_{sh} on radiation intensity of the sun or environmental humidity. I_{ph} strongly affected by solar radiation intensity, its value will vary with solar radiation. The intensity increases linearly [46]. The blocking currents I_0 and I_1 have an exponential relationship with temperature, their sensitivity is only affected by temperature and not by radiation intensity [47]. R_s and n_1, n_2 are highly sensitive to changes in solar radiation intensity and ambient temperature [48]. R_{sh} increases linearly with temperature and decreases with increasing solar radiation intensity. In this reference model, only the variation of radiation intensity of the sun and environmental humidity are considered, which are independent and do not affect each other [49].

$$
I_{ph} = \left[I_{ph,ref} + \alpha_{I_{sc}} \left(T - T_{ref} \right) \right] S / S_{ref}
\tag{4}
$$

Table 2
Information of internal parameters under the standard case (STC: temperature $= 33\ °C$, insolation $= 1000\ W/m^2$).

Parameter description	Numerical
$P_{pp}(Maximum\ power, W)$	60
$V_{mm}(Maximum\ voltage, V)$	17.1
$I_{mm}(Maximum\ current, A)$	3.5
$V_{oc}(Open\ circuit\ voltage, V)$	21.1
$I_{sc}(Short\ circuit\ current, A)$	3.8
$K_I(Current\ temperature\ coefficient, mA\ /°C)$	0.003
$K_V(Volatge\ temperature\ coefficient, mV\ /°C)$	-0.08

$$I_0 = I_{0,ref}\left(T/T_{ref}\right)^3 e^{\frac{q}{kn_1}\left(\frac{E_{g,ref}}{T_{ref}} - \frac{E_q}{T}\right)} \tag{5}$$

$$I_1 = I_{1,ref}\left(T/T_{ref}\right)^3 e^{\frac{q}{kn_2}\left(\frac{E_{g,ref}}{T_{ref}} - \frac{E_q}{T}\right)} \tag{6}$$

$$R_s = R_{s,ref} + \varepsilon_{R_s}\left(T - T_{ref}\right) + \gamma_{R_s}\left(S - S_{ref}\right) \tag{7}$$

$$R_{sh} = \left(R_{sh,ref} + \delta_{R_{sh}}\left(T - T_{ref}\right)\right)S_{ref}\ /\ S \tag{8}$$

$$n_1 = n_{ref} + \varepsilon_n\left(T - T_{ref}\right) + \sigma_n\left(S - S_{ref}\right) \tag{9}$$

$$n_2 = n_{ref} + \varepsilon_n\left(T - T_{ref}\right) + \sigma_n\left(S - S_{ref}\right) \tag{10}$$

In the above Eqs. (4)–(10), $Eg(eV)$ indicates the gapping for thermal cells, S (W/m^2) means radiation intensity of the PV module exposed to the sun, ε_{R_s} (Ω/K), $\delta_{R_{sh}}$ (Ω/K), ε_n (1/K) are the temperature coefficients of the resistances R_s, R_{sh} and the ideality factor (n_1, n_2) respectively. δ_{R_s} (Ω × m^2/W) is the resistance R_s of the light radiance coefficient, σ_n (m^2/W) is light radiance coefficient of the ideality factors for two diodes. The subscript of '*ref*' represents the correlation coefficient under the standard test environment of STC. Table 2 displays the parameters of the specific array operating under STCs. The PV model is made up of multiple arrays, consisting of 36 components connected in a series and 5 components connected in parallel. This composition is discussed throughout the research.

3. The model of photovoltaic module based on a DDM

This paper selects some operating conditions near or at STC as reference conditions. When work conditions are non-STC, like in lower radiance, the accuracy of parameter estimation decreases. Temperature and irradiation intensity continually vary. Using the traditional circuit model, the estimated parameter values also change constantly, resulting in non-fixed error values. This traditional method is complex and has low universality, which is not conducive to accurately estimating the parameter information inside the model. This paper modified and reconstructed the circuit model, and an improved model that is independent of the external environment and suitable for any operating conditions is proposed. Regardless of how much the temperature and irradiation intensity change, the estimated parameter values remain fixed, significantly improving the precision. The complexity is reduced and universality is stronger.

According to Eqs. (4)–(10), the parameters that need to be estimated by PV module are not only related to the solar radiation intensity and ambient temperature under the reference model, but also related to some referenced data. For the purpose of eliminating some the influence of referenced data on models accuracy, this section modifies and reconstructs the relationship between the parameter values of the model and the solar radiation intensity, ambient temperature.

Photocurrent generation I_{ph} is proportional to temperature and radiation intensity. As in the mathematical form in Eq. (4), we can convert it to Eq. (11).

$$I_{ph} = \left(I_{ph,ref}/S_{ref} - \alpha_{I_{sc}}T_{ref}\right) \cdot S + \alpha_{I_{sc}} \cdot ST$$

In Eq. (11), it can be seen that in addition to temperature and irradiance of the sun, there are some irrelevant elements. To further eliminate the influence of irrelevant values, Eq. (11) can be further transformed into Eq. (12). The unknown parameters A and B are included in the following equation.

$$I_{ph} = A \cdot S + B \cdot ST$$

According to the comparison of Eqs. (11) and (12), the units of A and B can be set as ($A \bullet m^2/W$) and ($A \bullet m^2/(W \bullet K)$), the values of

A and B can be equivalent to $I_{ph,ref}/S_{ref} - \alpha_{I_{sc}} T_{ref}/S_{ref}$ and $\alpha_{I_{sc}}/S_{ref}$.

For saturation current I_0 and diffusion current I_1, to eliminate the influence of irrelevant values, we can convert Eqs. (5) and (6) into Eqs. (13) and (14).

$$I_0 = CT^3 e^{-\frac{q\,\mathrm{Eg}}{kn_1 T}}$$

$$I_1 = C_1 T^3 e^{-\frac{q\,\mathrm{Eg}}{kn_2 T}}$$

As can be seen from Eqs. (13) and (14), the values of C and C_1 can be regarded as two unknown parameters, which take the values $I_{0,ref}/\left((T_{ref})^3 e^{-\frac{q\,\mathrm{E_{g,ref}}}{kn_1 T_{ref}}} \right)$ and $I_{1,ref}/\left((T_{ref})^3 e^{-\frac{q\,\mathrm{E_{g,ref}}}{kn_2 T_{ref}}} \right)$ respectively. The value of the energy model is critical to the processing of any device and can be applied to most battery models. An explanation of E_g is dependence on the environment is given in Ref. [50].

$$\mathrm{E_g}(T) = \mathrm{E_g}(0) - \left(\frac{\alpha T^2}{T + \beta} \right)$$

In the above equation, $E_g(0)$ represents the value of the band gap of the material at a temperature of $0K$ (in Calvin). The values of α and β are a constant, and then different values are used in the research process of different scholars. In Ref. [50], $E_g(0) = 1.1557eV$ was used, β was 1108 K. In Ref. [51], $E_g(0) = 1.166eV$ was used, β was 636 K. The continuous development of PV module materials should use different $E_g(0)$ values to calculate different models, it is not appropriate to use a fixed value to calculate all models. Therefore Eq. (15) is rewritten as Eq. (16).

$$\mathrm{E_g}(T) = D - \left(\frac{ET^2}{T + F} \right)$$

In Eq. (16), three unknown parameters (D, E, F) are included, and their three units are (eV) (eVK^{-1}) (K). The values of these three parameters are obtained by continuous fitting and optimization of experiment test data and calculation data, so that the accuracy of unknown parameters under different operating conditions and model changes can be improved.

As the shunt resistance R_{sh} indicates the leaking currents at both the p-n junction and gap edge of the diode. In this research, R_{sh} considered to be proportional to the radiation intensity inversely, it has a linear relationship with the change in temperature. Ignoring some of the components in Eq. (8), it can be rewritten as Eq. (17).

$$R_{sh} = \frac{G + H \cdot T}{S}$$

In Eq. (17), G and H are regarded as the information of two unknown parameters. G takes the value $(R_{sh,ref} - \delta_{R_{sh}} T_{ref}) \bullet S_{ref}$ and the unit is ($\Omega \cdot W/m^2$). H takes the value $\delta_{R_{sh}} \bullet S_{ref}$ and the unit is ($\Omega \cdot W/(m^2 \cdot K)$).

Finally, the work content of this paper is that the ideality factor (n_1, n_2) and series resistance R_s of the diode are also considered to be in a certain mathematical form with the solar radiation intensity and ambient temperature. So we can convert Eqs. (7), (9) and (10) into Eqs. (18)–(20).

$$R_s = J + L \cdot T + M \cdot S$$

$$n_1 = N_1 + O_1 \cdot T + P_1 \cdot S$$

$$n_2 = N_2 + O_2 \cdot T + P_2 \cdot S$$

In Eqs. (18)–(20), J (Ω) can take the value $R_{s,ref} - \varepsilon_{R_s} T_{ref} - \gamma_{R_s} S_{ref}$. N_1 and N_2 are the compensation parameters of the two ideality factors respectively, and both take the value of $n_{ref} - \varepsilon_n T_{ref} - \sigma_n S_{ref}$. L (Ω/K) and M ($\Omega \cdot m^2/W$) respectively take the value of ε_{R_s} and γ_{R_s}. O_1 (1/K) and O_2 (1/K) are both equal to ε_n. P_1 (m^2/W) and P_2 (m^2/W) can respectively be assigned as σ_n.

By utilizing Eqs. (12)–(20), the initial seven unknown parameters for estimation are transformed into eighteen unknown parameters $\Gamma = (A, B, C, C_1, D, E, F, G, H, J, L, M, N_1, N_2, O_1, O_2, P_1, P_2)$. Although the number of positional parameters of Γ is large, the advantage of this method is that it can be applied to all working conditions and can work normally under different solar radiation intensity and ambient temperature. In the new transformation equation, the likelihood parameter is constructed using real measured I-V data under physical conditions. Although Γ is generated by fitting in a single data, the value of Γ will not be influenced from original workspace, it

Table 3
Eight strategies for calculating the matrix $B_{i,G}$ in the QUATRE algorithm.

No.	QUATRE/B	Equation
1	QUATRE/best/1	$B_{i,G} = X_{gbest,G} + F \cdot \left(X_{r_1,G} - X_{r_2,G} \right)$
2	QUATRE/rand/1	$B_{i,G} = X_{r_0,G} + F \cdot \left(X_{r_1,G} - X_{r_2,G} \right)$
3	QUATRE/target/1	$B_{i,G} = X_{i,G} + F \cdot \left(X_{r_1,G} - X_{r_2,G} \right)$
4	QUATRE/target-to-rand/1	$B_{i,G} = X_{i,G} + F \cdot \left(X_{r_0,G} - X_{i,G} \right) + F \cdot \left(X_{r_1,G} - X_{r_2,G} \right)$
5	QUATRE/target-to-best/1	$B_{i,G} = X_{i,G} + F \cdot \left(X_{gbest,G} - X_{i,G} \right) + F \cdot \left(X_{r_1,G} - X_{r_2,G} \right)$
6	QUATRE/target/2	$B = X_{i,G} + F \cdot \left(X_{r_1,G} - X_{r_2,G} \right) + F \cdot \left(X_{r_3,G} - X_{r_4,G} \right)$
7	QUATRE/rand/2	$B = X_{r_0,G} + F \cdot \left(X_{r_1,G} - X_{r_2,G} \right) + F \cdot \left(X_{r_3,G} - X_{r_4,G} \right)$
8	QUATRE/best/2	$B = X_{gbest,G} + F \cdot \left(X_{r_1,G} - X_{r_2,G} \right) + F \cdot \left(X_{r_3,G} - X_{r_4,G} \right)$

is more universal.

4. Fitness function

Based on the above modified and reconstructed model parameters, the objective function aims to minimize the error between the measured current data supplied by the manufacturer and the current computed using unknown parameters that are obtained through the optimization algorithm. In this paper, *RMSE* [52,53] is used estimate accuracy of the parameter estimation of the PV module. As the value decreases, the estimated parameters tend to have a higher accuracy. The RMSE value is defined in Eq. (21).

$$RMSE(x) = \sqrt{\frac{1}{N_o} \sum_{i=1}^{N_o} f\ (V,I,x)^2}$$

where N_o denotes the volume of data for the I-V curve. Eq. (22) gives the expression for the definition of $f(V,I,x)$. Under different operating conditions, the original seven unknown parameters in the PV module can be converted into eighteen unknown parameters, the conversion of the two is expressed in Eq. (23). Parameter set Γ is not affected by the reference conditions, it is independent of the parameters under the reference conditions and applies to all operating conditions.

$$f(V,I,x) = I_{ph} - I_0 \left[exp \left(\frac{q(V + R_s I)}{n_1 kT} \right) - 1 \right] - I_1 \left[exp \left(\frac{q(V + R_s I)}{n_2 kT} \right) - 1 \right] - \frac{V + R_s I}{R_{sh}} - I$$

$$\begin{cases} x = \{ I_{ph}, I_0, I_1, R_s, R_{sh}, n_1, n_2 \} \\ \qquad\qquad \Downarrow \\ \Gamma = \{ A, B, C, C_1, D, E, F, G, H, J, L, M, N_1, N_2, O_1, O_2, P_1, P_2 \} \end{cases}$$

For the purpose of quantifying the accuracy of the proposed model, Individual absolute error (*IAE*) are also used as an additional performance metric in this research. It defined by the follow Eq. (24).

$$IAE = |Exp - Real|$$

where, *Exp* is the calculated value of the model and *Real* is the real value.

5. QUasi-Affine TRansformation evolutionary framework with cooperative structure and its improved

5.1. QUATRE algorithm

The QUATRE algorithm is an effective evolutionary method that has been proposed in 2016. In geometry, the mapping from *X* to *Y* space generally adopts a fixed mapping method. The evolution method of this algorithm simulates the imitation transformations from mathematics. The position update equation inside the algorithm is shown as Eq. (25).

$$\widehat{X} = \overline{M} \bigotimes \hat{X} + M \bigotimes B$$

In the above Eq. (25), $\widehat{X}$ is the basic matrix for the individuals in the population. $\widehat{X} = (X_1, X_2, ..., X_i, ..., X_{ps}), i \in [1, ps]$, *ps* represents the size of the population. *B* denotes evolution guidance matrix, *M* means a cooperative framework for population evolution. $\overline{M}$ is the

correlation matrix of M. The j dimension of the i individual is represented by $\widehat{X}_{i,G}$, and the corresponding population matrix is $\widehat{X}_G = [X_{1,G}, X_{2,G}, ..., X_{i,G}, ..., X_{ps,G},]$. $\otimes$ is represents multiplying operator according to the number of digits. There are many ways to generate the evolution guidance matrix $\overline{M}$. The evolution guidance vectors $B_{i,G}$ of each individual $X_{i,G}$ have a one-to-one correspondence. Table 3 gives several common representations of $B_{i,G}$. Among them. r_0, r_1, r_2, r_3, and r_4 all represent the individual position index array in the entire population.

There are several ways to generate the index sequence. The first is random selection under limited conditions, the second is full permutation selection, and the third is random offset selection. The QUATRE algorithm is based on the matrix evolution module, which uses the index generation method of full permutation selection. $X_{i,G}$ and $X_{gbest,G}$ are expressed as the target individually and the optimized one in the population at the time of iteration reaches the Gth time. The generation method of M is transformed from the initial M_{init}. We assume that $ps = D$, the M_{init} represents the matrix of lower triangularity with number of 1. Eq. (26) gives the transformation method of the matrix M_{init}.

$$M_{init} = \begin{bmatrix} 1 & & & \\ 1 & 1 & & \\ & & \cdots & \\ 1 & 1 & \cdots & 1 \end{bmatrix} \sim \begin{bmatrix} 1 & 1 & & \\ & \cdots & & \\ 1 & 1 & \cdots & 1 \\ & & 1 & \end{bmatrix} = M$$

This transformation is achieved by two consecutive operations:

- Randomly arrange all the elements in all row vectors in matrix M_{init}.
- Randomly arrange all row vectors of the modified matrix in the above step.

After the above-mentioned two-step matrix operations, the matrix M_{init} can be converted into a cooperative evolution matrix M. Pseudo-code 1 gives the flow steps of the QUATRE algorithm.

Algorithm 1 QUATRE algorithm Pseudo-code display

1: Input: Search space $[X_{max}, X_{min}]$, maximum fitness function evaluation times $MaxFes$, test function $F(x_i)$, search dimension D and population number ps.
2: Output: The optimal value $f(X_{gbest,d})$, the vector $X_{gbest,d}$ of the optimal solution, and the number of calls nfe of the function.
3: for i = 1; i ≤ ps; i++ **do**
4: Use the fitness function to evaluate the fitness value $F_{Xi,d}$ of the individuals in the population
5: end for
6: The evaluation number nfe of the population changes from 0 to ps.
7: Mark the population optimal value $F_{gbest,d}$ and the optimal solution position $X_{gbest,G}$.
8: While $nfe < nfe_{max}$ or $\delta f > eps$
9: Generate co-evolution matrix M according to Eq. (26).
10: for i = 1; i ≤ ps; i++ **do**
11:
$$B_{i,G} = X_{gbest,G} + F \cdot (X_{r_1,G} - X_{r_2,G})$$
12: end for
13:
$$\widehat{X}_{tmp} \leftarrow \overline{M} \otimes \widehat{X}_G + M \otimes B$$
14: Calculate the fitness evaluation value $f(\widehat{X}_{G+1})$ of the individual population.
15: $nfe = nfe + ps$
16: for i = 1; i ≤ ps; i++
17: if $f(X_{i,G}) > f(X_{i,tmp})$ **do**
18: $X_{i,G} = X_{i,tmp}$
19: end if
20: end for
21: Mark the optimal value $F_{gbest,d}$ and the position $X_{gbest,G}$ for solutions of the optimum
22: G = G + 1
23: end while
24: return output value

5.2. Reorganized QUATRE algorithm

A new QUATRE method based on the reorganization strategy (RQUATRE) is proposed in this section. The reorganized mechanism is based on the partial transformation of the population. In the process of iterative change of the population, the global best candidate solution and the historical optimal solution of each individual guide the position change of the solution. This process promotes the change of the population to completely tend to a better position. Such a process is often the direction with the fastest convergence rate, and the biggest problem will lead to the problem of falling into the local optimum.

We can use the fitness values of the individuals in the population to be sorted after each iteration, then recalculate and assign values to the individuals with lower rankings, and generate new individuals according to the worse situation to increase the variety of solutions.

Table 4
Details for the algorithmic coefficients.

Algorithm	Parameters settings
RQUATRE	$F = 0.7$
QUATRE	$F = 0.7$
PSO	$c_1 = 2, c_2 = 2, \omega = [0.9, 0.4]$
GWO	$a = [2, 0]$
FMO	$a = [-1, -2]$
PIO	$R = 0.2$

Table 5
RQUATRE and PSO, FMO, GWO comparison performance.

	PSO			FMO			GWO		
	Mean	Std	Min	Mean	Std	Min	Mean	Std	Min
F_1	$\textbf{4.00} \times \textbf{10}^\textbf{3}$	5.30×10^3	1.06×10^2	$\textbf{2.53} \times \textbf{10}^\textbf{10}$	3.09×10^9	1.90×10^{10}	$\textbf{1.12} \times \textbf{10}^\textbf{9}$	8.45×10^8	4.56×10^7
F_2	$\textbf{2.28} \times \textbf{10}^\textbf{15}$	7.66×10^{15}	2.53×10^5	$\textbf{7.51} \times \textbf{10}^\textbf{35}$	1.85×10^{36}	9.32×10^{31}	$\textbf{2.21} \times \textbf{10}^\textbf{31}$	9.47×10^{31}	1.78×10^{17}
F_3	$\textbf{3.11} \times \textbf{10}^\textbf{2}$	6.00×10^0	3.03×10^2	$\textbf{5.67} \times \textbf{10}^\textbf{4}$	6.89×10^3	4.47×10^4	$\textbf{3.17} \times \textbf{10}^\textbf{4}$	1.29×10^4	1.08×10^4
F_4	$\textbf{4.86} \times \textbf{10}^\textbf{2}$	2.23×10^1	4.05×10^2	$\textbf{3.05} \times \textbf{10}^\textbf{3}$	1.05×10^3	1.87×10^3	$\textbf{5.47} \times \textbf{10}^\textbf{2}$	3.65×10^1	4.83×10^2
F_5	6.23×10^2	2.01×10^1	5.81×10^2	$\textbf{8.39} \times \textbf{10}^\textbf{2}$	1.81×10^1	8.09×10^2	5.84×10^2	1.95×10^1	5.38×10^2
F_6	$\textbf{6.17} \times \textbf{10}^\textbf{2}$	1.05×10^1	6.01×10^2	$\textbf{6.74} \times \textbf{10}^\textbf{2}$	3.97×10^0	6.68×10^2	$\textbf{6.05} \times \textbf{10}^\textbf{2}$	2.66×10^0	6.01×10^2
F_7	7.91×10^2	1.82×10^1	7.56×10^2	$\textbf{1.23} \times \textbf{10}^\textbf{3}$	3.60×10^1	1.16×10^3	8.23×10^2	2.86×10^1	7.76×10^2
F_8	8.99×10^2	1.55×10^1	8.62×10^2	$\textbf{1.08} \times \textbf{10}^\textbf{3}$	1.64×10^1	1.04×10^3	8.84×10^2	2.75×10^1	8.49×10^2
F_9	2.25×10^3	1.21×10^3	9.01×10^2	$\textbf{7.95} \times \textbf{10}^\textbf{3}$	8.82×10^2	6.39×10^3	1.55×10^3	6.10×10^2	9.81×10^2
F_{10}	3.94×10^3	7.06×10^2	2.49×10^3	$\textbf{7.90} \times \textbf{10}^\textbf{3}$	4.83×10^2	6.77×10^3	3.97×10^3	7.79×10^2	2.67×10^3
F_{11}	$\textbf{1.20} \times \textbf{10}^\textbf{3}$	3.17×10^1	1.15×10^3	$\textbf{3.20} \times \textbf{10}^\textbf{3}$	5.39×10^2	2.57×10^3	$\textbf{1.36} \times \textbf{10}^\textbf{3}$	1.47×10^2	1.22×10^3
F_{12}	$\textbf{2.82} \times \textbf{10}^\textbf{5}$	3.93×10^5	3.78×10^4	$\textbf{4.27} \times \textbf{10}^\textbf{9}$	1.42×10^9	2.36×10^9	$\textbf{2.36} \times \textbf{10}^\textbf{7}$	1.88×10^7	2.46×10^5
F_{13}	$\textbf{1.61} \times \textbf{10}^\textbf{5}$	8.08×10^5	1.44×10^3	$\textbf{1.26} \times \textbf{10}^\textbf{9}$	3.94×10^8	5.45×10^8	$\textbf{3.18} \times \textbf{10}^\textbf{5}$	3.35×10^5	3.72×10^4
F_{14}	$\textbf{6.90} \times \textbf{10}^\textbf{3}$	5.48×10^3	1.63×10^3	$\textbf{6.06} \times \textbf{10}^\textbf{5}$	3.97×10^5	6.30×10^4	$\textbf{1.28} \times \textbf{10}^\textbf{5}$	2.33×10^5	2.47×10^3
F_{15}	$\textbf{8.72} \times \textbf{10}^\textbf{3}$	7.88×10^3	1.65×10^3	$\textbf{1.11} \times \textbf{10}^\textbf{7}$	4.36×10^6	3.21×10^6	$\textbf{2.36} \times \textbf{10}^\textbf{5}$	6.94×10^5	1.29×10^4
F_{16}	2.42×10^3	1.98×10^2	2.12×10^3	$\textbf{3.90} \times \textbf{10}^\textbf{3}$	2.31×10^2	3.23×10^3	2.35×10^3	2.25×10^2	1.90×10^3
F_{17}	2.09×10^3	1.98×10^2	1.87×10^3	$\textbf{2.56} \times \textbf{10}^\textbf{3}$	1.59×10^2	2.23×10^3	1.99×10^3	1.58×10^2	1.79×10^3
F_{18}	$\textbf{1.73} \times \textbf{10}^\textbf{5}$	1.03×10^5	4.26×10^4	$\textbf{4.43} \times \textbf{10}^\textbf{6}$	2.58×10^6	1.19×10^6	$\textbf{5.66} \times \textbf{10}^\textbf{5}$	7.57×10^5	7.12×10^4
F_{19}	7.78×10^3	6.64×10^3	1.97×10^3	$\textbf{8.74} \times \textbf{10}^\textbf{7}$	5.05×10^7	1.40×10^7	$\textbf{3.82} \times \textbf{10}^\textbf{5}$	3.97×10^5	7.93×10^3
F_{20}	2.35×10^3	1.29×10^2	2.21×10^3	$\textbf{2.69} \times \textbf{10}^\textbf{3}$	1.08×10^2	2.45×10^3	2.29×10^3	1.00×10^2	2.14×10^3
F_{21}	2.42×10^3	2.23×10^1	2.37×10^3	$\textbf{2.60} \times \textbf{10}^\textbf{3}$	2.01×10^1	2.56×10^3	2.38×10^3	3.36×10^1	2.35×10^3
F_{22}	2.87×10^3	1.31×10^3	2.30×10^3	5.06×10^3	3.52×10^2	4.34×10^3	2.90×10^3	9.76×10^2	2.35×10^3
F_{23}	$\textbf{2.88} \times \textbf{10}^\textbf{3}$	5.10×10^1	2.80×10^3	$\textbf{3.09} \times \textbf{10}^\textbf{3}$	3.59×10^1	3.03×10^3	2.75×10^3	3.76×10^1	2.70×10^3
F_{24}	$\textbf{3.01} \times \textbf{10}^\textbf{3}$	5.73×10^1	2.90×10^3	$\textbf{3.32} \times \textbf{10}^\textbf{3}$	3.78×10^1	3.25×10^3	2.93×10^3	3.33×10^1	2.88×10^3
F_{25}	$\textbf{2.89} \times \textbf{10}^\textbf{3}$	1.36×10^1	2.88×10^3	$\textbf{3.47} \times \textbf{10}^\textbf{3}$	1.13×10^2	3.32×10^3	$\textbf{2.95} \times \textbf{10}^\textbf{3}$	3.27×10^1	2.90×10^3
F_{26}	3.99×10^3	1.32×10^3	2.80×10^3	$\textbf{7.57} \times \textbf{10}^\textbf{3}$	8.17×10^2	6.08×10^3	4.40×10^3	3.72×10^2	3.64×10^3
F_{27}	$\textbf{3.26} \times \textbf{10}^\textbf{3}$	3.48×10^1	3.21×10^3	$\textbf{3.53} \times \textbf{10}^\textbf{3}$	7.42×10^1	3.38×10^3	3.20×10^3	2.93×10^{-4}	3.20×10^3
F_{28}	3.22×10^3	2.16×10^1	3.19×10^3	4.34×10^3	2.13×10^2	4.01×10^3	$\textbf{3.32} \times \textbf{10}^\textbf{3}$	4.15×10^1	3.29×10^3
F_{29}	$\textbf{3.80} \times \textbf{10}^\textbf{3}$	2.04×10^2	3.40×10^3	$\textbf{5.04} \times \textbf{10}^\textbf{3}$	2.15×10^2	4.58×10^3	3.42×10^3	9.93×10^1	3.21×10^3
F_{30}	$\textbf{7.56} \times \textbf{10}^\textbf{3}$	1.89×10^3	5.71×10^3	$\textbf{2.14} \times \textbf{10}^\textbf{8}$	6.93×10^7	8.90×10^7	$\textbf{2.12} \times \textbf{10}^\textbf{5}$	2.04×10^5	1.73×10^4

The number of individuals that reorganize the sorted population needs to be discussed. If a fixed number of changes is determined, the fixed number of changes is always guaranteed from the beginning of the iteration to the end, which ensures the diversity of candidate solutions, but does not guarantee the effectiveness of population changes. If the number of candidate solutions that the population needs to change is change, it will become two directions, one is from less to more, the other is from more to less. We use the trend of change from more to less, it can ensure that the change direction of the candidate solutions will increase at the beginning of the iteration. The individuals in the population avoid dropping to any local optimum to a large extent in the later stages by iterating.

In this paper, the exact amount of candidate solutions $k = ceil(ps/10)$ that are required to change is location, where *ceil* represents the round-up operator. Amount for candidate solutions varies with the increasing iterations. Eq. (27) gives details of the variation procedure.

$$\omega_\alpha = \frac{k-1}{Max-1}(\alpha-1)+1,$$

where ω_α means amount of candidate solutions to be reassigned during the α iteration, $1 \ll \omega \ll k$, *Max* represents for the maximally iterative amount of algorithm running.

Table 6
RQUATRE and QUATRE, PIO comparison performance.

	QUATRE			RQUATRE			PIO		
	Mean	Std	Min	Mean	Std	Min	Mean	Std	Min
F_1	$\mathbf{2.75 \times 10^3}$	1.06×10^3	1.15×10^3	1.00×10^2	1.55×10^{-4}	1.00×10^2	$\mathbf{8.97 \times 10^8}$	5.41×10^8	2.15×10^8
F_2	$\mathbf{4.70 \times 10^{32}}$	7.92×10^{32}	2.06×10^{28}	1.50×10^7	7.61×10^7	2.00×10^2	$\mathbf{1.10 \times 10^{30}}$	5.84×10^{30}	2.65×10^{20}
F_3	$\mathbf{2.13 \times 10^5}$	5.14×10^4	1.20×10^5	3.00×10^2	1.74×10^{-1}	3.00×10^2	$\mathbf{6.90 \times 10^4}$	2.29×10^4	3.70×10^4
F_4	4.23×10^2	2.76×10^{-1}	4.23×10^2	4.36×10^2	2.85×10^1	4.00×10^2	$\mathbf{6.84 \times 10^2}$	6.76×10^1	5.85×10^2
F_5	$\mathbf{6.34 \times 10^2}$	1.07×10^1	6.07×10^2	6.32×10^2	3.06×10^1	5.87×10^2	$\mathbf{6.84 \times 10^2}$	3.19×10^1	5.95×10^2
F_6	6.00×10^2	1.69×10^{-4}	6.00×10^2	6.02×10^2	3.25×10^0	6.00×10^2	$\mathbf{6.49 \times 10^2}$	1.01×10^1	6.30×10^2
F_7	$\mathbf{8.67 \times 10^2}$	9.89×10^0	8.46×10^2	8.54×10^2	3.18×10^1	7.98×10^2	$\mathbf{9.44 \times 10^2}$	5.14×10^1	8.52×10^2
F_8	$\mathbf{9.34 \times 10^2}$	1.07×10^1	9.12×10^2	9.13×10^2	2.34×10^1	8.75×10^2	$\mathbf{9.47 \times 10^2}$	2.65×10^1	8.99×10^2
F_9	9.00×10^2	2.00×10^{-1}	9.00×10^2	2.52×10^3	1.11×10^3	1.05×10^3	4.31×10^3	9.10×10^2	3.02×10^3
F_{10}	$\mathbf{6.51 \times 10^3}$	2.88×10^2	6.04×10^3	4.28×10^3	4.29×10^2	3.43×10^3	$\mathbf{5.62 \times 10^3}$	5.85×10^2	4.45×10^3
F_{11}	$\mathbf{1.16 \times 10^3}$	7.49×10^0	1.14×10^3	1.15×10^3	1.89×10^1	1.12×10^3	$\mathbf{1.48 \times 10^3}$	7.99×10^1	1.35×10^3
F_{12}	$\mathbf{2.01 \times 10^7}$	8.76×10^6	5.14×10^6	1.27×10^5	2.46×10^5	1.37×10^4	$\mathbf{4.56 \times 10^7}$	6.11×10^7	3.57×10^6
F_{13}	$\mathbf{5.34 \times 10^5}$	2.68×10^5	1.19×10^5	2.86×10^3	3.20×10^3	1.37×10^3	$\mathbf{3.48 \times 10^5}$	1.13×10^6	1.82×10^4
F_{14}	1.49×10^3	7.32×10^0	1.48×10^3	1.88×10^3	5.62×10^2	1.44×10^3	$\mathbf{1.50 \times 10^5}$	1.91×10^5	3.99×10^3
F_{15}	$\mathbf{1.95 \times 10^4}$	1.54×10^4	6.78×10^3	1.83×10^3	4.23×10^2	1.52×10^3	$\mathbf{3.09 \times 10^4}$	1.59×10^4	9.30×10^3
F_{16}	$\mathbf{2.69 \times 10^3}$	2.04×10^2	2.19×10^3	2.68×10^3	3.29×10^2	1.96×10^3	$\mathbf{3.06 \times 10^3}$	3.16×10^2	2.50×10^3
F_{17}	1.92×10^3	1.10×10^2	1.77×10^3	2.10×10^3	1.75×10^2	1.79×10^3	$\mathbf{2.27 \times 10^3}$	1.85×10^2	1.95×10^3
F_{18}	$\mathbf{1.70 \times 10^5}$	6.01×10^4	8.39×10^4	3.91×10^4	4.69×10^4	5.25×10^3	$\mathbf{6.05 \times 10^5}$	4.85×10^5	8.58×10^4
F_{19}	1.98×10^3	1.38×10^1	1.95×10^3	1.27×10^4	1.88×10^4	1.91×10^3	$\mathbf{1.34 \times 10^6}$	1.36×10^6	1.25×10^5
F_{20}	2.13×10^3	6.02×10^1	2.04×10^3	2.46×10^3	1.72×10^2	2.17×10^3	$\mathbf{2.57 \times 10^3}$	1.71×10^2	2.32×10^3
F_{21}	$\mathbf{2.44 \times 10^3}$	8.21×10^0	2.43×10^3	2.43×10^3	3.88×10^1	2.35×10^3	$\mathbf{2.47 \times 10^3}$	3.23×10^1	2.41×10^3
F_{22}	$\mathbf{7.11 \times 10^3}$	1.39×10^1	4.21×10^3	5.43×10^3	1.17×10^3	2.30×10^3	3.33×10^3	1.65×10^3	2.44×10^3
F_{23}	2.79×10^3	1.09×10^1	2.77×10^3	2.81×10^3	4.37×10^1	2.73×10^3	3.05×10^3	9.01×10^1	2.88×10^3
F_{24}	$\mathbf{3.00 \times 10^3}$	1.01×10^1	2.98×10^3	3.00×10^3	5.04×10^1	2.92×10^3	3.14×10^3	7.73×10^1	3.03×10^3
F_{25}	2.88×10^3	1.64×10^{-2}	2.88×10^3	2.88×10^3	1.22×10^0	2.88×10^3	3.03×10^3	5.22×10^1	2.97×10^3
F_{26}	$\mathbf{4.70 \times 10^3}$	9.76×10^1	4.44×10^3	4.50×10^3	6.65×10^2	2.90×10^3	5.71×10^3	1.45×10^3	3.68×10^3
F_{27}	3.20×10^3	6.00×10^{-5}	3.20×10^3	3.20×10^3	1.62×10^{-4}	3.20×10^3	3.50×10^3	1.01×10^2	3.35×10^3
F_{28}	3.30×10^3	1.26×10^{-4}	3.30×10^3	3.30×10^3	1.68×10^{-4}	3.30×10^3	3.44×10^3	7.48×10^1	3.32×10^3
F_{29}	3.91×10^3	1.29×10^2	3.63×10^3	3.65×10^3	1.98×10^2	3.23×10^3	4.46×10^3	3.21×10^2	3.75×10^3
F_{30}	$\mathbf{2.70 \times 10^4}$	1.83×10^4	6.24×10^3	3.24×10^3	1.71×10^1	3.21×10^3	8.09×10^6	4.75×10^6	1.40×10^6

6. Results and discussions

During the experiment, we evaluated the performance of PSO, FMO, GWO, PIO, QUATRE, and RQUATRE algorithms on the CEC2017 test suite using Matlab2020b software. The experiment was performed using an individual laptop computer equipped with the Windows 10 operating system. The experiment was aimed at comparing the effectiveness of each algorithm.

6.1. Description and experimental analysis on test functions

The CEC2017 test suite is used as a basis for evaluating different algorithms, but in *F_2 has been omitted due to its inconsistent behavior, particularly in higher dimensions, and significant performance fluctuations when implemented in Matlab, C. The specific descriptive information of the CEC2017 test suite is given in literature [54]. The CEC2017 test suite contains exactly 30 test functions, each of which will be described in detail below.

The single-peak functions (F_1–F_3) have a single global optimal point and are designed to test the algorithm's capacity for global search. Simple multimodal functions (F_4–F_{10}) have only one globally optimum point and multiple locally optimum positions, testing the algorithm's capacity to explore the global optimal position despite being affected by local optimal positions. In considering algorithms to solve practical optimization problems using hybrid functions (F_{11}–F_{20}), various components of variances exhibit diverse characteristics. About composition functions (F_{21}–F_{30}), the variable is partitioned randomly into smaller sub-components, with each sub-component utilizing distinct basis functions. Global optimal candidate solution is attained by identifying the local optima with the lowest deviation value. This function design facilitates the fusion of sub-function characteristics and ensures continuity around local and global optima.

During the following experiments, an evaluation of the iterative performance in the RQUATRE algorithm will be made and contrasted with five of the most advanced evolutionary algorithms, namely QUATRE, PSO, FMO, GWO, PIO. There are some random factors in the meta-heuristic algorithm. For fairness, candidate solutions, dimensions, and running times of all algorithms are kept highly consistent. For the candidate solutions the number is defined as 100, the dimension of the test function is 50, each experiment was run 50 times, and the maximum fitness function evaluation times was set to 2.5×10^5. The specific values and settings of other parameters in each algorithm are given in Table 4.

The RQUATRE algorithm and five state-of-the-art algorithms are experimentally simulated on the classic CEC 2017 test suite. To avoid the chance factor and randomness of the experimental results, this paper independently runs 50 experiments on 30 test functions for these six algorithms. The data in Tables 5 and 6 shows the final convergence accuracy of the algorithm. In the process of running the

Table 7
In terms of mean, the number of wins of RQUATRE.

Algorithm	Unimodal	Multimodal	Hybrid	Composition	Win	Ranking
RQUATRE VS FMO	3	7	10	9	29	1
RQUATRE VS PIO	3	7	10	9	29	1
RQUATRE VS QUATRE	3	4	6	8	21	2
RQUATRE VS PSO	3	2	6	6	17	3
RQUATRE VS GWO	3	2	7	3	15	4

(a) Function F_1 (b) Function F_2 (c) Function F_3 (d) Function F_4

(e) Function F_5 (f) Function F_6 (g) Function F_7 (h) Function F_8

(i) Function F_9 (j) Function F_{10} (k) Function F_{11} (l) Function F_{12}
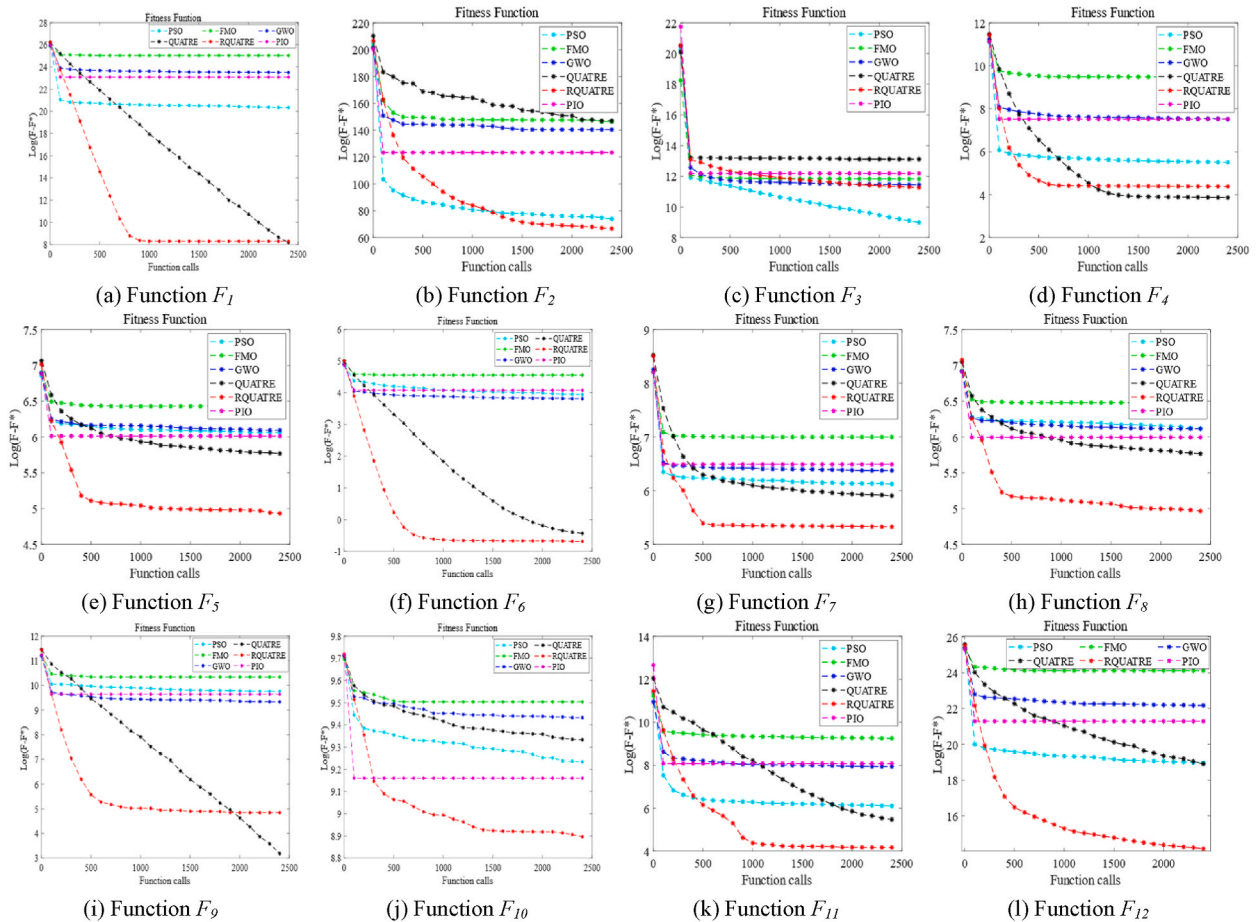
Fig. 3. (a)–(l) represent speed of convergence graphs for the comparison algorithm for both function F_1–F_{12}, respectively.

algorithm 50 times, the final convergence value (optimal value) obtained by each algorithm on each test function was recorded. Mean, Std and Min values of the algorithm were also recorded for multiple runs. Mean is the most commonly used and representative indicator in statistics, which represents the central tendency of the data set distribution. The performance of the algorithm mainly depends on the Mean, and the smaller its value, the better the algorithm achieves. In Tables 5 and 6, if the Mean of the RQUATRE algorithm is lower than that of the other algorithms, the value is marked as bold. As can be seen from the tables, the bolded values are overwhelming. Table 7 also counts the amount of winners and the ranking comparison between the RQUATRE algorithm and five evolutionary algorithms with respect to the four baseline functions. Compared with the FMO and PIO algorithms, the RQUATRE algorithm has 29 wins on the 30 test functions, and its performance ranks first. The RQUATRE algorithm outperformed the QUATRE algorithm in 21 functions and ranked second in terms of performance. RQUATRE outperforms PSO and GWO algorithms by 17 and 15 times respectively, which is exceeding by half for the baseline test set. Judging from these the experiment data, the RQUATE algorithm has strong competitiveness in finding the global optimal solution.

Fig. 3(a–l) displays the rate for convergence of various algorithms on functions F_1–F_{12}, respectively. Fig. 4(a–r) shows the speed of convergence behavior in functions F_{13}–F_{30}. As seen from all the curves, the RQUATRE algorithm converges to a smaller value and achieves better results than the QUATRE algorithm, except for three functions, F4, F9, and F14. At the same time, PSO algorithm is considered to be the most competitive meta-heuristic algorithms, since the algorithm is easier to understand and has powerful globally
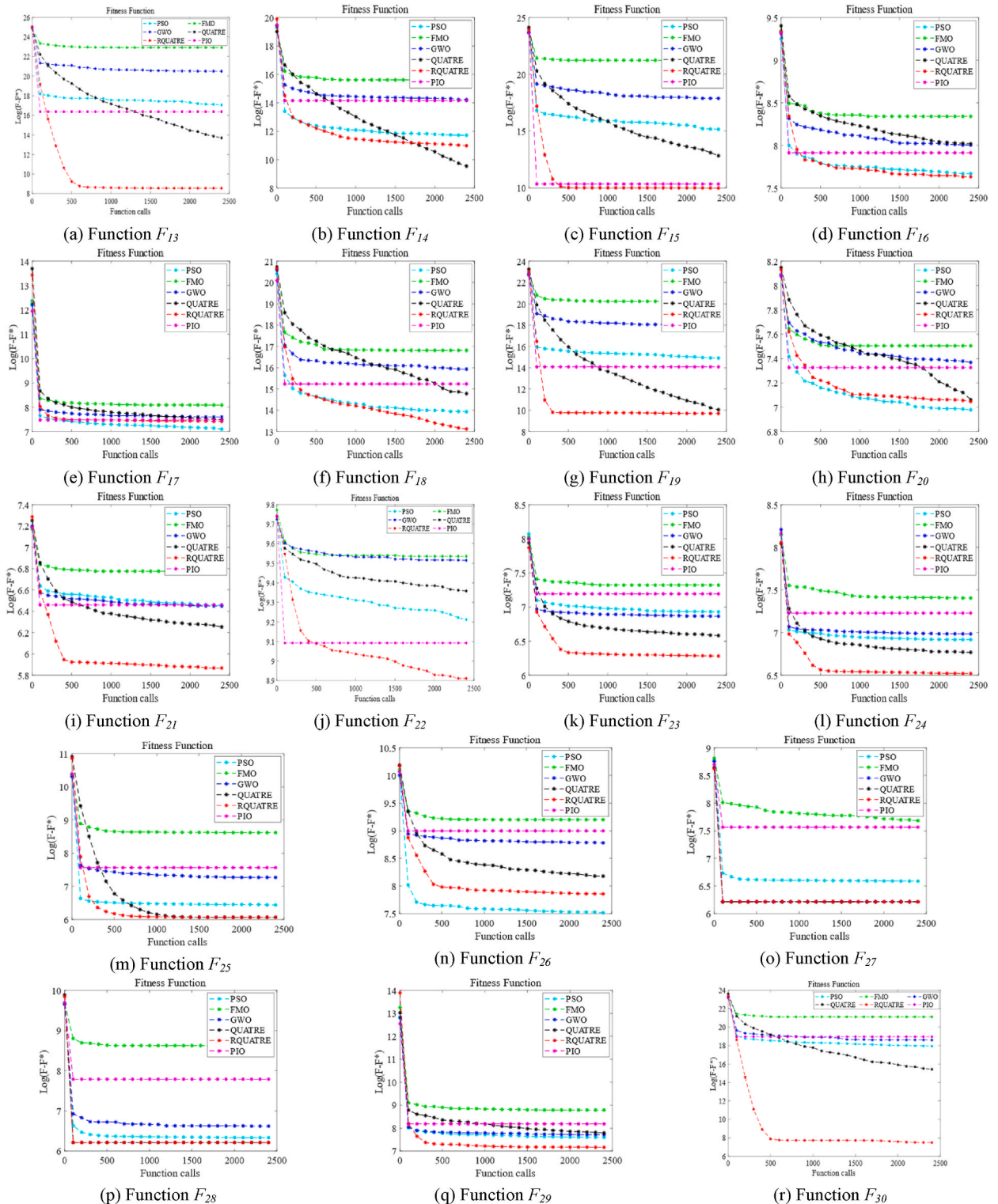
Fig. 4. (a)–(r) represent speed of convergence graphs for the comparison algorithm for both function F_{13}–F_{30}, respectively.

seeking properties.

Excluding the four test functions F_3, F_{17}, F_{20}, and F_{26}, the proposed RQUATRE algorithm outperforms PSO among other remaining test functions. In comparison with the algorithms of FMO, PIO and GWO, RQUATRE basically converges to the best value on the 30 test

Table 8
Setting ranges for eighteen unknown parameters in PV module.

Parameters	Lower limit of value	Upper limit of value
A (A·m^2/W)	0	$10^{-3} \times \left(150\% \times I_{sc,STC} - \alpha_{I_{sc}} T_{STC}\right)$
B (A·m^2/(W·K))	0	$10^{-2} \times \alpha_{I_{sc}}$
C	0	10^4
C_1	0	10^4
D (eV)	0.5	1.5
E (eVK^{-1})	0	0.01
F (K)	0	10^5
G (Ω·W/m^2)	$\left(\dfrac{V_{mm,STC}}{I_{sc,STC} - I_{mm,STC}} - 0.298\right) \times 10^3$	10^8
H (Ω·W/(m^2·K))	-100	0
J (Ω)	-1.298	$\dfrac{V_{oc,STC} - V_{mm,STC}}{I_{mm,STC}} + 0.298$
L (Ω/K)	0	10^{-3}
M (Ω·m^2/W)	-10^{-3}	10^{-3}
N_1	-0.5	5.98
O_1 (1/K)	-0.01	0
P_1 (m^2/W)	-10^{-3}	10^{-3}
N_2	-0.5	5.98
O_2 (1/K)	-0.01	0
P_2 (m^2/W)	-10^{-3}	10^{-3}

Table 9
The optimal estimation parameters of various algorithms on the PV module and their corresponding *RMSE* values.

Parameter	PSO	FMO	GWO	RQUATRE	QUATRE	PIO
A (A·m^2/W)	9.25×10^{-4}	-5.79×10^0	-2.88×10^1	0.00×10^0	0.00×10^0	0.00×10^0
B (A·m^2/(W·K))	6.08×10^{-7}	1.02×10^0	9.67×10^{-2}	0.00×10^0	0.00×10^0	3.25×10^{-9}
C	4.94×10^3	2.00×10^{-1}	2.23×10^1	3.64×10^2	2.54×10^2	1.62×10^2
C_1	5.16×10^3	-4.90×10^0	-1.05×10^0	6.36×10^2	2.54×10^2	1.40×10^2
D (eV)	1.36×10^0	-6.61×10^0	8.40×10^1	7.44×10^{-1}	1.03×10^0	9.68×10^{-1}
E (eVK^{-1})	3.94×10^{-3}	-6.70×10^0	-1.58×10^4	7.14×10^{-3}	5.55×10^{-3}	4.54×10^{-3}
F (K)	5.36×10^4	1.16×10^1	-6.03×10^1	3.79×10^4	4.57×10^4	6.16×10^3
G (Ω·W/m^2)	7.84×10^7	6.12×10^4	-6.98×10^6	1.00×10^8	1.00×10^8	6.68×10^7
H (Ω·W/(m^2·K))	-4.26×10^1	-1.60×10^1	-1.01×10^3	-2.35×10^{-1}	0.00×10^0	0.00×10^0
J (Ω)	-4.62×10^{-1}	-5.00×10^0	-5.26×10^0	-3.10×10^{-1}	-3.98×10^{-1}	-3.61×10^{-1}
L (Ω/K)	5.24×10^{-4}	2.60×10^0	-5.38×10^0	4.16×10^{-4}	4.94×10^{-4}	6.04×10^{-4}
M (Ω·m^2/W)	1.13×10^{-4}	-4.57×10^0	1.07×10^0	1.25×10^{-4}	1.23×10^{-5}	-1.09×10^{-5}
N_1	1.67×10^0	7.17×10^0	1.21×10^0	1.84×10^0	2.92×10^0	1.99×10^0
O_1 (1/K)	-4.63×10^0	4.16×10^0	2.16×10^2	-5.41×10^{-3}	-5.49×10^{-3}	-5.33×10^{-3}
P_1 (m^2/W)	-2.23×10^{-5}	3.34×10^0	-3.84×10^2	7.84×10^{-5}	-7.58×10^{-5}	3.92×10^{-5}
N_2	1.83×10^0	6.61×10^0	2.08×10^2	3.06×10^0	3.49×10^0	2.28×10^0
O_2 (1/K)	-5.26×10^{-3}	1.44×10^0	8.36×10^1	-5.89×10^{-3}	-5.43×10^{-3}	-5.67×10^{-3}
P_2 (m^2/W)	1.92×10^{-4}	3.88×10^0	2.51×10^2	7.35×10^{-5}	-1.56×10^{-4}	-3.44×10^{-5}
RMSE	9.72×10^{-1}	1.87×10^6	4.62×10^{-1}	2.99×10^{-3}	3.08×10^{-3}	1.04×10^{-2}

functions. Overall, the RQUATRE algorithm converges to the minimum value on most of the 30 test functions, and its performance is excellent. The curves in Figs. 3 and 4 show that the RQUATRE algorithm fluctuates more at the beginning of the iteration and less in the later part of the iteration. The rate of decline for curves indicates that with an increasing iteration rate, the poorer individuals among the population can mutate in position, what can have an effect on increasing the species diversity and then move themselves to a better position by communication or jump the locally optimal limit for moving to a better location. The RQUATRE algorithm has good convergence speed and convergence accuracy. As a result, an excellent balance of algorithm exploration and exploitation is achieved during the iterative process.

6.2. Result of improved model of PV module

In this subsection, the RQUATRE algorithm is applied to the parameter estimation of the PV module. The manufacturer conducts a series of experiments on a 57 mm commercial silicon R.T.C. French solar cell under fixed environmental conditions ($T = 33\,^\circ$C, $G = 1000$ W/m^2) to obtain the I-V data set used in this paper. Table 8 gives the range of the parameter set Γ.

To obtain the estimated performance of physical parameters under different operating conditions, the value of parameter set Γ will not change, regardless of the reference conditions at that time. We optimized the parameter set Γ by using empirical I-V datasets with diverse fitted profiles, while a feasibility optimal approach is needed to estimates the specific values of the calculated parameter set Γ.

RQUATRE algorithm and several other algorithms to compare the information of the estimation parameter, the RQUATRE algorithm obviates for the premature narrow convergence and poor convergence accuracy problems.

Table 10
Measured data, calculated data and IAE for photovoltaic module.

Data set	Actual data		Calculated data				
	V (V)	I (A)	I_c (A)	IAE (I)	P (W)	P_c (W)	IAE (P)
1	−0.2057	0.764	0.763016	0.000984	−0.15715	−0.15695	0.000202
2	−0.1291	0.762	0.762109	0.000109	−0.09837	−0.09839	1.41×10^{-5}
3	−0.0588	0.7605	0.763158	0.002658	−0.04472	−0.04487	0.000156
4	0.0057	0.7605	0.765612	0.005112	0.004335	0.004364	2.91×10^{-5}
5	0.0646	0.76	0.757081	0.002919	0.049096	0.048907	0.000189
6	0.1185	0.759	0.757066	0.001934	0.089942	0.089712	0.000229
7	0.1678	0.757	0.75707	6.95E-05	0.127025	0.127036	1.17×10^{-5}
8	0.2132	0.757	0.757902	0.000902	0.161392	0.161585	0.000192
9	0.2545	0.7555	0.756145	0.000645	0.192275	0.192439	0.000164
10	0.2924	0.754	0.754591	0.000591	0.22047	0.220642	0.000173
11	0.3269	0.7505	0.750808	0.000308	0.245338	0.245439	0.000101
12	0.3585	0.7465	0.748862	0.002362	0.26762	0.268467	0.000847
13	0.3873	0.7385	0.742258	0.003758	0.286021	0.287477	0.001455
14	0.4137	0.728	0.728301	0.000301	0.301174	0.301298	0.000125
15	0.4373	0.7065	0.710904	0.004404	0.308952	0.310878	0.001926
16	0.459	0.6755	0.67996	0.00446	0.310055	0.312102	0.002047
17	0.4784	0.632	0.634849	0.002849	0.302349	0.303712	0.001363
18	0.496	0.573	0.576037	0.003037	0.284208	0.285714	0.001506
19	0.5119	0.499	0.49988	0.00088	0.255438	0.255888	0.00045
20	0.5265	0.413	0.417271	0.004271	0.217445	0.219693	0.002249
21	0.5398	0.3165	0.313118	0.003382	0.170847	0.169021	0.001825
22	0.5521	0.212	0.217876	0.005876	0.117045	0.120289	0.003244
23	0.5633	0.1035	0.110008	0.006508	0.058302	0.061968	0.003666
24	0.5736	−0.01	−0.00986	0.00014	−0.00574	−0.00566	8.01×10^{-5}
25	0.5833	−0.123	−0.12413	0.001127	−0.07175	−0.0724	0.000657
26	0.59	−0.21	−0.20955	0.000451	−0.1239	−0.12363	0.000266
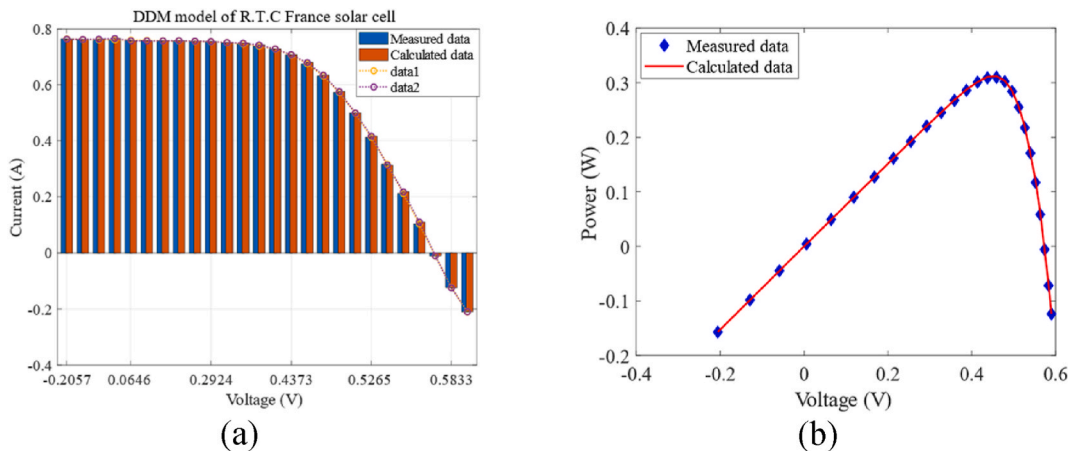
Fig. 5. Comparison between the measured data and calculated data of the RQUATRE algorithm in PV module. (a) is I-V characteristic convergence curves and (b) represents the characteristic convergence curves of P-V.

In the experiment, the size, dimension, and iteration number of the candidate solutions are consistent with the above algorithm experiments. To validate the robustness of RQUATRET, the five algorithms of PSO, FMO, GWO, QUATRE, and PIO are still applied to photovoltaic module estimation of parameters. It is displayed in Table 9 that the estimation results and RMSE obtained for parameters solution set Γ. With the smaller values of RMSE, there is a more accurate estimation of the parameters. It is observed that the *RMSE* values obtained by the RQUATRE algorithm and the QUATRE algorithm are 2.99×10^{-3} and 3.08×10^{-3} respectively. The units of magnitude of the two are the same, both are 10^{-3}, but the *RMSE* values obtained by the RQUATRE algorithm is much lower. Compared with the other four algorithms, the *RMSE* value of the RQUATRE algorithm is also the lowest. The parameters estimated by the RQUATRE algorithm is the most accurate. The values of PSO and GWO do not differ much, and their accuracy is similar for the estimation of parameters. The *RMSE* value of the FMO algorithm is 1.87×10^6, with the largest error value, which has the worst performance. According to the evaluation *RMSE* of parameter estimation, RQUATRE obtained the best estimated parameter value.

Table 10 presents a collection of the actual I-V data, along with the respective calculated data and the absolute errors for each individual value. The variables represent the real input I and V in the PV module. Once the parameter set has been successfully
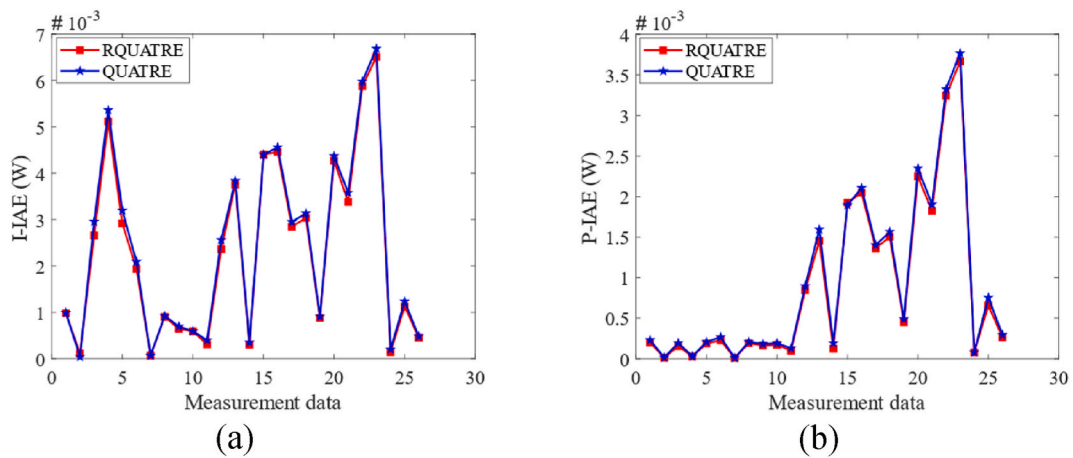
Fig. 6. Individual absolute error of QUATRE and RQUATRE in PV module. (a) is IAE values of current and (b) represents IAE values of power.
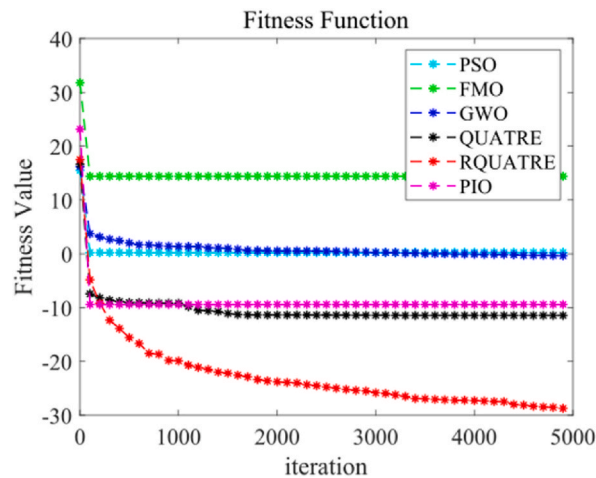
Fig. 7. Individual absolute error of QUATRE and RQUATRE in PV module.

estimated, the output current I_c can be computed, and the actual power values P and the corresponding calculated power values P_c may also be determined. In Table 10, it is observed that photovoltaic modules with current IAE does not exceed 0.00650842, and the power IAE does not exceed 0.00366619. Both current and power IAE values are very smaller, which indicating that the input current and voltage are basically fitted with the output current and voltage calculated after parameter estimation. Fig. 5(a and b) demonstrate a close similarity between the measured current data and the calculated current data. Additionally, the I-V and P-V curves exhibit a high degree of fitting accuracy. This shows that the parameters estimated by the RQUATRE algorithm are quite accurate. To verify that the improved algorithm outperforms the original algorithm, another experiment was also performed. Fig. 6(a and b) plots the IAE value curves obtained by estimating parameters from the RQUATRE and QUATRE algorithms. The blue pentagram-shaped curve represents the QUATRE algorithm, while the red square-shaped curve represents the RQUATRE algorithm. It can be observed that whether it is current IAE or power IAE, the blue curve is above the red curve as a whole, the individual absolute error of the QUATRE algorithm is higher than that of RQUATRE on most data points. This also fully shows that the RQUATRE algorithm has achieved satisfactory results in the parameter estimation of the PV module.

The convergence plots for all algorithms are displayed in Fig. 7. As shown in the figure, RQUATRE achieves both the fastest convergence rates and highest accuracy for seeking the optimal solution compared to other five algorithms. Moreover, the RQUATRE algorithm displays stronger potential for obtaining optimal values. Based on the experiments and discussions mentioned earlier, the RQUATRE algorithm is more persuasive in parameter estimation and can attain superior fitness function values.

7. Conclusion

We first present an effective QUATRE algorithm with recombination mechanism (RQUATRE) in this paper. The reorganization mechanism can continuously rearrange the candidate solutions that are ranked low in the algorithm, which can effectively overcome

the drawback that the convergence precision of QUATRE algorithm is too low. Second, we also propose a nominated approach to evaluate the properties with different reference and working situations for photovoltaic modules, using as a novel conversion method to simulate the dependence of the physical parameters in the photovoltaic module on the optimization model. For the improvement of the algorithm and model proposed in this paper, we made the following experiments. Firstly, the RQUATRE algorithm was evaluated on the CEC2017 test suite with five other heuristics. The performance of the simulation experiment demonstrates the excellence of the improved algorithms. Secondly, the improvement of photovoltaic models was experimented on the basis of known messages from the manufacturer's provided parameters estimation work. The experimental data indicate that the parameter information for an improved version of the module estimated by the RQUATRE algorithm becomes far more accurately, and the values of RMSE and IAE reach more satisfactory values compared to the previous work.

Although the content of the work in this study has certain research results, there are still elements that need to be improved in the future work. Firstly, in terms of algorithm improvement, this study added a reorganization mechanism to the RQUTRE algorithm, which improves its convergence precision and avoids it falling into the local optimum trap, but does not reduce the complexity by which it can be increased in future work. Secondly, for the double-diode of PV model, this study expands seven parameters into eighteen parameters, which causes the difficulty of dimensional curse and poses a higher challenge. For the meta-heuristic algorithm for solving similar issues, the eighteen parameters information consist of exactly what reflects the properties by the algorithm as proposed on our research. The improved PV model causes the problem of dimensionality curse, and the dimensionality of the problem can be reduced appropriately in the content of future work.

Author contribution statement

Fei-Fei Liu: Conceived and designed the experiments; Performed the experiments; Analyzed and interpreted the data; Contributed reagents, materials, analysis tools or data; Wrote the paper.

Shu-Chuan Chu: Conceived and designed the experiments.

Chia-Cheng Hu: Analyzed and interpreted the data.

Junzo Watada: Conceived and designed the experiments; Analyzed and interpreted the data.

Jeng-Shyang Pan: Performed the experiments; Analyzed and interpreted the data; Contributed reagents, materials, analysis tools or data.

Data availability statement

Data associated with this study has been deposited at http://www.sandia.gov/pv/docs/Database.htm.

Declaration of competing interest

The authors declare that they have no known competing financial interests or personal relationships that could have appeared to influence the work reported in this paper.

[3]; [45].

References

[1] B. Desalegn, D. Gebeyehu, B. Tamirat, Wind energy conversion technologies and engineering approaches to enhancing wind power generation: a review, Heliyon (2022), e11263.

[2] R. Abbassi, A. Abbassi, M. Jemli, S. Chebbi, Identification of unknown parameters of solar cell models: a comprehensive overview of available approaches, Renew. Sustain. Energy Rev. 90 (2018) 453–474.

[3] H. Ibrahim, N. Anani, Variations of pv module parameters with irradiance and temperature, Energy Proc. 134 (2017) 276–285.

[4] N. Ammari, M. Mehdi, A.A. Merrouni, H. El Gallassi, E. Chaabelasri, A. Ghennioui, Experimental study on the impact of soiling on the modules temperature and performance of two different pv technologies under hot arid climate, Heliyon 8 (11) (2022), e11395.

[5] K. Ishaque, Z. Salam, An improved modeling method to determine the model parameters of photovoltaic (pv) modules using differential evolution (de), Sol. Energy 85 (9) (2011) 2349–2359.

[6] H.A. Kazem, J.H. Yousif, M.T. Chaichan, A.H. Al-Waeli, K. Sopian, Long-term power forecasting using frnn and pca models for calculating output parameters in solar photovoltaic generation, Heliyon 8 (1) (2022), e08803.

[7] M.A.G. De Brito, L. Galotto, L.P. Sampaio, G.d.A. e Melo, C.A. Canesin, Evaluation of the main mppt techniques for photovoltaic applications, IEEE Trans. Ind. Electron. 60 (3) (2012) 1156–1167.

[8] Y. Ando, T. Oku, M. Yasuda, K. Ushijima, H. Matsuo, M. Murozono, Dependence of electric power flow on solar radiation power in compact photovoltaic system containing sic-based inverter with spherical si solar cells, Heliyon 6 (1) (2020), e03094.

[9] K. Nabil, N. Moubayed, R. Outbib, General review and classification of different MPPT techniques, Renew. Sustain. Energy Rev. 68 (2017) 1–18.

[10] G.M. Tina, F.B. Scavo, Energy performance analysis of tracking floating photovoltaic systems, Heliyon 8 (8) (2022), e10088.

[11] M.B. Rhouma, A. Gastli, L.B. Brahim, F. Touati, M. Benammar, A simple method for extracting the parameters of the pv cell single-diode model, Renew. Energy 113 (2017) 885–894.

[12] J.D. Bastidas-Rodriguez, G. Petrone, C.A. Ramos-Paja, G. Spagnuolo, A genetic algorithm for identifying the single diode model parameters of a photovoltaic panel, Math. Comput. Simulat. 131 (2017) 38–54.

[13] H. Rezk, S. Ferahtia, A. Djeroui, A. Chouder, A. Houari, M. Machmoum, M.A. Abdelkareem, Optimal parameter estimation strategy of PEM fuel cell using gradient-based optimizer, Energy 239 (2022), 122096.

[14] F. Attivissimo, F. Adamo, A. Carullo, A.M.L. Lanzolla, F. Spertino, A. Vallan, On the performance of the double-diode model in estimating the maximum power point for different photovoltaic technologies, Measurement 46 (9) (2013) 3549–3559.

[15] D. Allam, D. Yousri, M. Eteiba, Parameters extraction of the three diode model for the multi-crystalline solar cell/module using moth-flame optimization algorithm, Energy Convers. Manag. 123 (2016) 535–548.

[16] J.-S. Pan, A.-Q. Tian, V. Snášel, L. Kong, S.-C. Chu, Maximum power point tracking and parameter estimation for multiple-photovoltaic arrays based on enhanced pigeon-inspired optimization with Taguchi method, Energy 251 (2022), 123863.

[17] A.-Q. Tian, S.-C. Chu, J.-S. Pan, Y. Liang, A novel pigeon-inspired optimization based mppt technique for pv systems, Processes 8 (3) (2020) 356.

[18] V. Jately, B. Azzopardi, J. Joshi, A. Sharma, S. Arora, et al., Experimental analysis of hill-climbing mppt algorithms under low irradiance levels, Renew. Sustain. Energy Rev. 150 (2021), 111467.

[19] X. Li, H. Wen, Y. Hu, Y. Du, Y. Yang, A comparative study on photovoltaic mppt algorithms under en50530 dynamic test procedure, IEEE Trans. Power Electron. 36 (4) (2020) 4153–4168.

[20] Y.-P. Huang, S.-Y. Hsu, A performance evaluation model of a high concentration photovoltaic module with a fractional open circuit voltage based maximum power point tracking algorithm, Comput. Electr. Eng. 51 (2016) 331–342.

[21] R.H. Tan, P.L. Tai, V. Mok, Solar irradiance estimation based on photovoltaic module short circuit current measurement, in: 2013 IEEE International Conference on Smart Instrumentation, Measurement and Applications (ICSIMA), IEEE, 2013, pp. 1–4.

[22] W. De Soto, S.A. Klein, W.A. Beckman, Improvement and validation of a model for photovoltaic array performance, Sol. Energy 80 (1) (2006) 78–88.

[23] F. Ghani, M. Duke, J. Carson, Numerical calculation of series and shunt resistances and diode quality factor of a photovoltaic cell using the lambert w-function, Sol. Energy 91 (2013) 422–431.

[24] A. Acevedo-Luna, A. Morales-Acevedo, Study of validity of the single-diode model for solar cells by i–v curves parameters extraction using a simple numerical method, J. Mater. Sci. Mater. Electron. 29 (18) (2018) 15284–15290.

[25] A. Elkholy, A. Abou El-Ela, Optimal parameters estimation and modelling of photovoltaic modules using analytical method, Heliyon 5 (7) (2019), e02137.

[26] D.S. Chan, J.C. Phang, Analytical methods for the extraction of solar-cell single-and double-diode model parameters from iv characteristics, IEEE Trans. Electron. Dev. 34 (2) (1987) 286–293.

[27] A. Elkholy, A. Abou El-Ela, Optimal parameters estimation and modelling of photovoltaic modules using analytical method, Heliyon 5 (7) (2019), e02137.

[28] W. Song, L. Lu, H. Chaomin, Generalized maximal utility for mining high average-utility itemsets, Knowl. Inf. Syst. 63 (2021) 2947–2967.

[29] K. Wang, Y. Liu, D. Liu, Q. Shi, Improved particle swarm optimization algorithm based on Gaussian-grid search method, J. Inform. Hiding Multimedia Sig. Process. 9 (4) (2018) 1031–1037.

[30] Z. Meng, Y. Chen, X. Li, C. Yang, Y. Zhong, Enhancing quasi-affine transformation evolution (quatre) with adaptation scheme on numerical optimization, Knowl. Base Syst. 197 (2020), 105908.

[31] L. Song, X. Jiang, L. Wang, X. Hu, Monte Carlo node localization based on improved quarte optimization, J. Sens. 2021 (2021) 1–12.

[32] S. Mirjalili, Genetic algorithm, in: Evolutionary Algorithms and Neural Networks vol. 780, Springer, 2019, pp. 43–55.

[33] J.-S. Pan, P. Hu, S.-C. Chu, Binary fish migration optimization for solving unit commitment, Energy 226 (2021), 120329.

[34] S. Mirjalili, Dragonfly algorithm: a new meta-heuristic optimization technique for solving single-objective, discrete, and multi-objective problems, Neural Comput. Appl. 27 (4) (2016) 1053–1073.

[35] F.-F. Liu, S.-C. Chu, X. Wang, J.-S. Pan, A collaborative dragonfly algorithm with novel communication strategy and application for multithresholding color image segmentation, J. Internet Technol. 23 (1) (2022) 45–62.

[36] S. Mirjalili, S.M. Mirjalili, A. Lewis, Grey wolf optimizer, Adv. Eng. Software 69 (2014) 46–61.

[37] E. Kaya, B. Gorkemli, B. Akay, D. Karaboga, A review on the studies employing artificial bee colony algorithm to solve combinatorial optimization problems, Eng. Appl. Artif. Intell. 115 (2022), 105311.

[38] J.-S. Pan, L.-G. Zhang, R.-B. Wang, V. Snášel, S.-C. Chu, Gannet optimization algorithm: a new metaheuristic algorithm for solving engineering optimization problems, Math. Comput. Simulat. 202 (2022) 343–373.

[39] J. Tu, H. Chen, M. Wang, A.H. Gandomi, The colony predation algorithm, J. Bionic Eng. 18 (3) (2021) 674–710.

[40] B. Shi, H. Ye, L. Zheng, J. Lyu, C. Chen, A.A. Heidari, Z. Hu, H. Chen, P. Wu, Evolutionary warning system for covid-19 severity: colony predation algorithm enhanced extreme learning machine, Comput. Biol. Med. 136 (2021), 104698.

[41] S. Mirjalili, A. Lewis, The whale optimization algorithm, Adv. Eng. Software 95 (2016) 51–67.

[42] Q. Feng, S.-C. Chu, J.-S. Pan, J. Wu, T.-S. Pan, Energy-efficient clustering mechanism of routing protocol for heterogeneous wireless sensor network based on bamboo forest growth optimization, Entropy 24 (7) (2022) 980.

[43] D. Yadav, O.P. Verma, Energy optimization of multiple stage evaporator system using water cycle algorithm, Heliyon 6 (7) (2020), e04349.

[44] R. Drummond, L.D. Couto, D. Zhang, Resolving Kirchhoff′s laws for parallel li-ion battery pack state-estimators, IEEE Trans. Control Syst. Technol. 30 (5) (2021) 2220–2227.

[45] O.D. Montoya, W. Gil-González, A MIQP model for optimal location and sizing of dispatchable DGs in DC networks, Energy Syst. 121 (2021) 181–202.

[46] T. Ma, W. Gu, L. Shen, M. Li, An improved and comprehensive mathematical model for solar photovoltaic modules under real operating conditions, Sol. Energy 184 (2019) 292–304.

[47] P. Singh, N.M. Ravindra, Temperature dependence of solar cell performance an analysis, Sol. Energy Mater. Sol. Cell. 101 (2012) 36–45.

[48] F. Bradaschia, M.C. Cavalcanti, A.J. do Nascimento, E.A. da Silva, G.M. de Souza Azevedo, Parameter identification for pv modules based on an environment-dependent double-diode model, IEEE J. Photovoltaics 9 (5) (2019) 1388–1397.

[49] S.P. Aly, S. Ahzi, N. Barth, An adaptive modelling technique for parameters extraction of photovoltaic devices under varying sunlight and temperature conditions, Appl. Energy 236 (2019) 728–742.

[50] Y.P. Varshni, Temperature dependence of the energy gap in semiconductors, Physica 34 (1) (1967) 149–154.

[51] I. Grekhov, New principles of high power switching with semiconductor devices, Solid State Electron. 32 (11) (1989) 923–930.

[52] M. Ćalasan, S.H.A. Aleem, A.F. Zobaa, On the root mean square error (rmse) calculation for parameter estimation of photovoltaic models: a novel exact analytical solution based on lambert w function, Energy Convers. Manag. 210 (2020), 112716.

[53] Y. Zhang, M. Ma, Z. Jin, Comprehensive learning jaya algorithm for parameter extraction of photovoltaic models, Energy 211 (2020) 118644.

[54] G. Wu, R. Mallipeddi, P.N. Suganthan, Problem Definitions and Evaluation Criteria for the Cec 2017 Competition on Constrained Real-Parameter Optimization, National University of Defense Technology, Changsha, Hunan, PR China and Kyungpook National University, Daegu, South Korea and Nanyang Technological University, Singapore, 2017. Technical Report.